

Molecular dynamics simulations of low-energy (25–200 eV) argon ion interactions with silicon surfaces: Sputter yields and product formation pathways

Nawoyuki A. Kubota and Demetre J. Economou^{a)}

Plasma Processing Laboratory, Department of Chemical Engineering, University of Houston, Houston, Texas 77204-4792

Steven J. Plimpton

Sandia National Laboratories, Albuquerque, New Mexico 87185

(Received 21 October 1997; accepted for publication 7 January 1998)

The etch yield and subsurface damage are important issues in low energy (<200 eV) ion interactions with surfaces. In particular, atomic layer etching requires etching of electronic materials with monolayer precision and minimal interlayer atomic mixing. In this study, the molecular dynamics technique is used to simulate the impact of argon ions on chlorine-free and chlorine-passivated silicon surfaces, under conditions relevant to atomic layer etching. Thousands of individual ion impact simulations are performed on a massively parallel supercomputer. The silicon sputter yield is obtained for Ar ion energies ranging from 25 to 200 eV. Where possible, simulation results are compared to available experimental data. Volatile product formation during ion bombardment of ordered surfaces tends to follow distinct local trajectories. For example, the formation of products due to 120 eV Ar ions impacting onto Si(001)(2×1) at normal incidence has been found to occur mainly by a mechanism in which the Ar ion impacts directly in-between a surface silicon dimer pair. The energetic recoiled silicon atoms undercut nearby silicon atoms resulting in product formation. Several other product formation pathways have also been observed.

© 1998 American Institute of Physics. [S0021-8979(98)03908-5]

I. INTRODUCTION

This article studies the interaction of low energy (25–200 eV) argon ions with surfaces using the molecular dynamics (MD) technique by focusing on the phenomena of sputtering and surface damage of bare and chlorine-passivated silicon. Such phenomena are important in atomic layer etching (ALET),^{1–7} and also in reactive ion etching (RIE) of microelectronic materials.⁸ In ALET, a single crystal surface with an adsorbed monolayer of halogen is exposed to argon ion bombardment. It is important to control the ion energy and dose to etch away the topmost layer of the crystal without damaging the layers underneath. In RIE, the surface is exposed to neutral atoms/molecules and ions simultaneously. Ion beam irradiation in the presence of a reactive halogen gas has been found to greatly increase the etch rate of silicon, versus the etch rate due to ion beam irradiation or halogen gas exposure alone.⁹ This sputter yield enhancement has been attributed to the presence of subsurface mixing^{10,11} and the decreased binding energy of halogenated silicon at the surface. Subsurface mixing does not occur under conditions conducive to ALET.

The only published MD study relevant to ALET that we are aware of is that of Athavale and Economou.¹² However, no reaction mechanisms were reported in that work. It will be asserted now, and illustrated later by MD simulations, that product ejection from defect-free surfaces bombarded by low

energy ions follows distinct pathways and correlates with impact location. In contrast to ALET, there are numerous MD studies related to RIE. Feil *et al.*¹³ have performed 200 eV impacts on Si and have observed the formation of tower-like structures which exhibit a large etch enhancement. Barone *et al.*¹⁴ have also observed similar surface roughened structures due to direct reactive ion etching of Si by 25 eV Cl⁺. Barone,¹⁵ and Barone and Graves¹⁶ have studied the etch mechanism of fluorinated silicon (fluorosilyl) layers. Helmer and Graves¹⁷ reported a study of fluorinated silicon surfaces impacted by energetic Si and SiF_x species.

Other works examine the defect formation of pristine surfaces bombarded by energetic species.^{18,19} The role of such damage is of particular concern in ALET¹² and in ion-assisted etching of microstructures and nano-structures.²⁰ Several other studies have also been conducted to examine the degree of damage produced during low energy ion irradiation.^{21–23} We will briefly address this issue in the context of the formation of steady-state disordered surface layers.

The theory of physical sputtering (no chemical reactions) has been formulated in the context of linear cascade theory,^{24,25} through which a series of collisions beneath the surface due to energetic particle impact eventually leads to ejection of atoms from the surface. At low energies, typically below 200 eV, linear cascade theory fails.²⁶ Several authors have provided modified yield expressions to account for the increasing importance of the lattice cohesive energy in reducing the yield at low ion impact energies.^{26,27} Furthermore,

^{a)}Electronic mail: economou@uh.edu

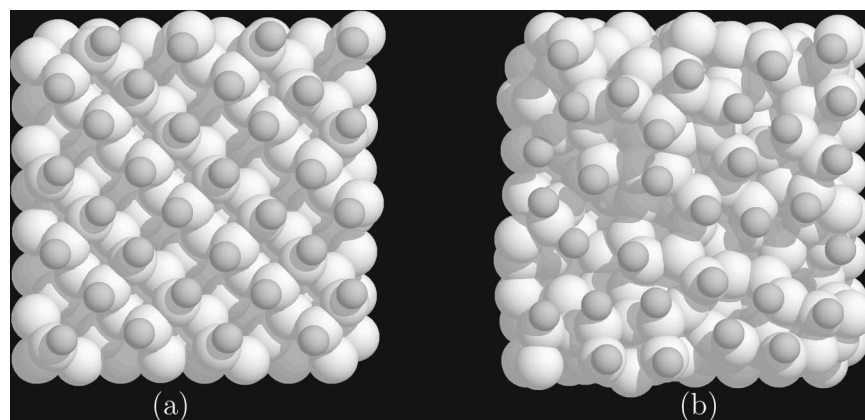


FIG. 1. (a) top view of a defect-free silicon lattice with 1 ML of chemisorbed chlorine. (b) top view of a silicon surface that was amorphized by 200 successive 50 eV Ar impacts and with Cl adsorbed after amorphization. For both (a) and (b), the smaller spheres represent chlorine atoms (not to scale).

at even lower energies, corrections due to the surface topology must be considered to describe sputtering.²⁸ Reaction product formation events resulting from these low energy ion impacts can be expected to be qualitatively simpler, involving several collisions over a range of only a few angstroms, of atoms mainly in the top atomic layers. For silicon sputtering by low energy argon ions, the sputter yield Y , defined as the number of silicon atoms removed per impacting ion, is expected to be $Y \approx 10^{-2}$ for argon energies near 100 eV. Balooch *et al.*²⁹ have reported physical sputtering yields for ion energies down to 120 eV in an experimental beam study, while yields down to 200 eV have been calculated in MD studies.^{13,16}

II. DESCRIPTION OF SIMULATION

The simulation procedure is conceptually similar to that used in other MD studies of ion-surface interactions.^{12,13,15,16,30–32} In the simulations, an initially defect-free (001)-oriented (2×1) reconstructed silicon lattice is generated and equilibrated at 300 K. The lattice is composed of nine atomic layers, or 288 silicon atoms. In simulations involving 200 eV Ar ions, 13 atomic layers are used. However, for the sake of simplicity, all references to lattices in this study will denote the nine atomic-layer configuration. The bottom two layers are fixed rigidly in space, while periodic boundary conditions are applied laterally to remove edge effects. Berendsen's heat removal scheme³³ with a coupling constant of 4 fs is applied to the lower 6 Å of the lattice. Figure 1(a) shows the top view of a defect-free silicon lattice with 1 ML of chlorine chemisorbed onto the surface. For this, and all other lattices with some degree of chlorine chemisorption, the silicon lattice is first equilibrated to 300 K, and then thermal-energy chlorine atoms are impacted onto the surface at random locations. Figure 1(a) shows the stabilization of the (2×1) surface reconstruction and the dimer "rows" and "channels."

To generate amorphized (damaged) surfaces, a defect-free surface is repeatedly and successively bombarded by normally incident argon ions at random locations on the lattice, similar to the method employed by Barone and Graves.¹⁶ Argon atoms are impacted onto the surface at in-

tervals of 2 ps without allowing long-time-scale processes such as annealing, recrystallization and defect diffusion to occur between impacts. Furthermore, any argon atoms remaining in the lattice after 2 ps are removed, after which heat removal is applied to the entire lattice, and then the lattice is re-equilibrated at 300 K for 0.5 ps prior to further argon impaction. Figure 1(b) shows the top view of a "steady-state" layer of the silicon lattice after successive bombardment by 200, 50 eV Ar ions, and then chlorine surface passivation.

Argon ions are assumed to impact the surface as neutrals of the same energy as the starting ion. The argon interactions are described by the Molière potential, while all other interactions utilize the silicon/chlorine parameterization of Feil *et al.*¹³ of the Stillinger–Weber interaction potentials for silicon.^{34–36} These potentials have been found to stabilize a bulk diamond lattice structure, as well as provide a satisfactory description of a (2×1) reconstructed surface. Integration is performed using the velocity form of Verlet's method^{15,37} with a step size of 3.83×10^{-16} s, or 1/200 of the Si–Si oscillation period. Although a constant time-step size was used in the present work, using an adaptive time-step size should improve the code efficiency.

Silicon sputter yields and product distributions are calculated by simulating thousands of normally incident energetic argon trajectories from different locations within a plane approximately 10 Å above the lattice. The argon position vectors within this plane are selected with a random number generator subroutine and included into the simulation input files. Unlike the procedure used to generate "amorphized" surfaces described above, ions are impacted onto the same initial lattice. This is in contrast to the study of Athavale and Economou¹² in which the surface was bombarded successively by argon ions as in the procedure used to generate amorphized surfaces. Having each ion bombard the same initial lattice, however, allows for use of a massively parallel supercomputer to simultaneously calculate thousands of ion impacts over the course of several hours. In particular, a single ion impact simulation is performed for approximately 1.2 ps on each node of a Sandia National Laboratory nCUBE-2 supercomputer. A total of 1024 nodes

per run are used for the parallel computation of 1023 ion impacts (the remaining node is used for “coordinating” the run). Further calculations are done using several HP 9000-735 125-MHz workstations.

Different classes of initial condition lattices are used in this study:

- (1) Defect-free bare silicon.
- (2) Defect-free silicon with 1 ML of chlorine coverage [shown in Fig. 1(a)].
- (3) Amorphized bare silicon.
- (4) Amorphized silicon with 1 ML of chlorine coverage [shown in Fig. 1(b)].

These lattices are impacted with argon ions having energy in the range 25–200 eV. Further impacts of 25, 37.5 and 50 eV ions on defect-free and amorphized surfaces with 0.25, 0.5 and 0.75 ML chlorine coverage are also performed to examine the sputtering yield trends with chlorine surface coverage.

Yields are determined from volatile products observed at the end of each impact simulation. Product species are defined as any atom or cluster of atoms which cross a plane 2 Å above the surface, where the surface is arbitrarily defined as the highest atomic position in the lattice prior to ion impact. Experience has shown that this provides an adequate criterion for product species, since large surface deformations have not been observed. Also, volatile species are observed to eject well within 0.5 ps after impact, consistent with similar studies by Athavale and Economou¹² and Smith *et al.*³⁸ Nevertheless, the product species are verified visually in case products are found at the end of the simulation near the surface plane. Visualization is performed using RasMol,³⁹ to create images for stills and animations. The contribution of sputtered silicon products due to the formation and subsequent desorption of weakly bound species has been found to be negligible due to the absence of chlorine incorporated beneath the surface, consistent with several simulation studies.^{12,15,16}

III. RESULTS AND DISCUSSION

A. Steady-state damage

Figure 2 shows the evolution of the radial distribution function $g(r)$ over the whole lattice after different doses of argon ions, starting from defect-free bare silicon. The main peaks correspond well to the $g(r)$ of a highly structured silicon lattice.⁴⁰ Notice that $g(r)$ does not vary significantly after 20 successive, 50 eV argon impacts, suggesting the approach to a steady-state near-surface amorphous layer expected in the presence of an appreciable flux of energetic ions. The semioordered nature of $g(r)$ after many impacts is due to the effect of a $g(r)$ calculation over a cell containing distinct amorphous and defect-free regions. Figure 3 shows the atomic density distribution $\rho(z)$ as a function of the position normal to the surface. This plot shows a clear amorphization of the top three atomic layers while leaving the lower layers virtually intact.

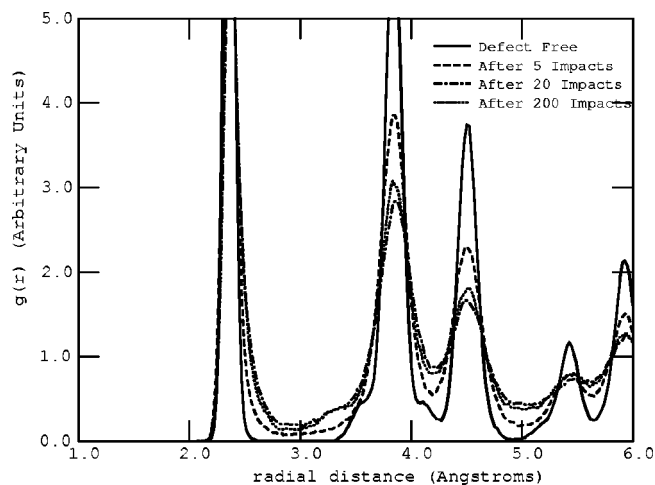


FIG. 2. Radial distribution function calculated over the entire simulation cell after 0, 5, 20, and 200 successive 50 eV Ar impacts on an initially defect-free bare silicon lattice.

B. Sputter yield and product distributions

Figure 4 shows a plot of the sputter yield of amorphized bare silicon versus the argon ion energy, compared with other computational^{13,16,38} and experimental^{29,41,42} sources of Si sputter yields as well as a plot of the yield estimate of Zalm.²⁶ There are very few sources of experimental yield data for comparison at the lower ion energies. However, at 120 and 200 eV, this MD study is in very good agreement with the experimental yields of Balooch *et al.*²⁹ and MD studies of Barone and Graves.¹⁶ Furthermore, the calculated yields are shown to correspond well to the yield estimates of Zalm,²⁶ down to 75 eV. Figure 5 shows a plot of sputter yield versus \sqrt{E} for this study. Very near the threshold energy, one expects a deviation from the square root dependence of yield on ion energy found by Steinbrüchel²⁷ and

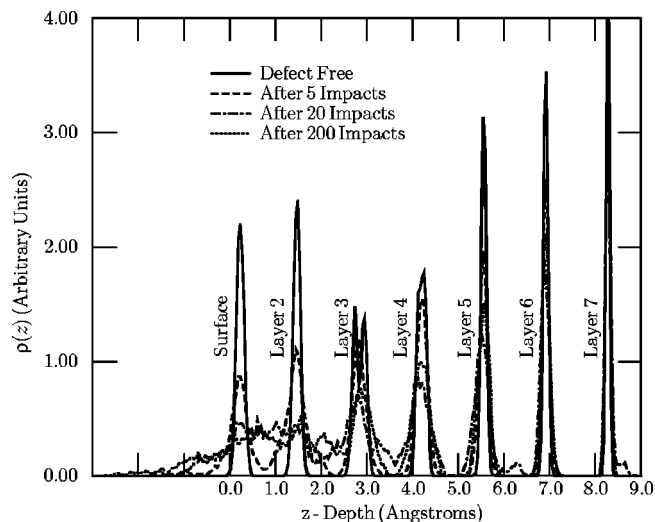


FIG. 3. The atomic density distribution as a function of vertical position z within the simulation cell after 0, 5, 20, and 200 successive 50 eV Ar impacts on an initially defect-free bare silicon lattice. This plot shows the apparent evolution towards a steady-state disordered surface region of the top three silicon layers.

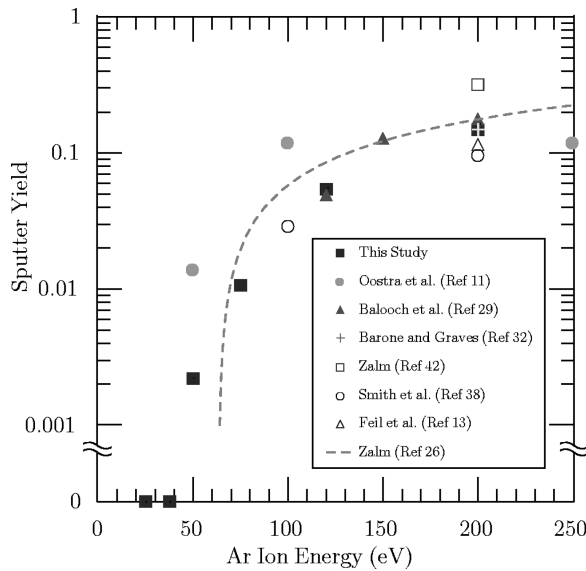


FIG. 4. Sputter yield Y_{Si} of amorphized bare silicon obtained from this study compared with several other reports.

Zalm.²⁶ Figure 5 reveals a threshold energy of approximately 37.5 eV, consistent with the work of Chang *et al.*,⁴³ extrapolating a threshold energy around 35 eV.

Table I lists the results of the various different sets of impact simulations performed for this study. Listed are the overall silicon sputter yield Y_{Si} and the total number of various observed silicon-containing species ejected, for different ion-energy and initial condition lattice combinations. The right-most column shows the total number of individual impact simulations performed in each set of impact simulations listed. One observation is the apparent yield enhancement of chlorine passivated surfaces versus non-passivated surfaces. This self-limiting silicon etch behavior is essential for ALET in which the presence of Cl at the surface dictates whether sputtering will or will not occur. For simulations with fractional monolayer Cl coverage, a generally increasing sputter yield is observed at higher coverages, as well as a larger

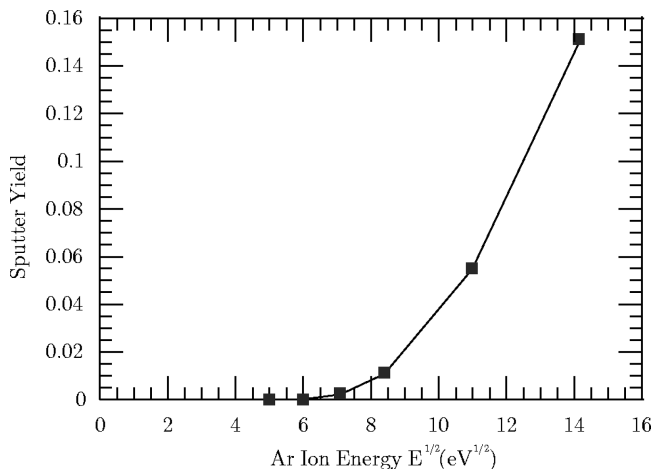


FIG. 5. Sputter yield Y_{Si} of amorphized bare silicon plotted vs \sqrt{E} for results of this study. This plot shows a threshold energy of about 37.5 eV. The sputter yield does not scale with \sqrt{E} near the threshold energy.

TABLE I. Tabulation of the silicon sputter yields and ejected product species as a function of ion impact energy, shown in the first column from left. The second column from left represents the lattice used (A=Amorphized, DF=Defect free). The third column from left lists the surface chlorine coverage in monolayers (ML). The tenth column from left tabulates the total number of silicon atoms from larger ($x \geq 3$) silicon-containing clusters.

E (eV)	Lat.	(ML)	Y_{Si}	SiCl ₃	SiCl ₂	SiCl	Si	Si ₂ Cl _x	Si _x Cl _y	Im- pacts
25	A	0	0	2046
25	A	1	0	2046
37.5	A	0	0	2046
37.5	A	0.25	0	2046
37.5	A	0.50	0	2046
37.5	A	0.75	0.002	...	2	2	2046
37.5	A	1	0.003	...	3	1	1533
50	DF	0	0	2046
50	DF	1	0.011	...	20	13	3069
50	A	0	0.002	4	1790
50	A	0.25	0.002	4	2045
50	A	0.50	0.005	...	1	3	6	2046
50	A	0.75	0.006	...	6	6	2046
50	A	1	0.003	...	7	2046
75	DF	0	0	1790
75	DF	1	0.037	...	49	30	...	2	...	2255
75	A	0	0.011	33	3068
75	A	0.25	0.021	20	23	2046
75	A	0.50	0.014	...	3	22	4	2046
75	A	0.75	0.023	...	7	31	8	2046
75	A	1	0.024	3	15	24	...	2	3	2046
120	DF	0	0.025	30	1216
120	DF	1	0.097	1	31	53	...	6	...	998
120	A	0	0.055	56	1023
120	A	1	0.085	2	33	39	5	4	...	1023
200	DF	0	0.080	84	1051
200	DF	1	0.171	...	17	100	3	11	7	873
200	A	0	0.151	227	2	...	1532
200	A	1	0.230	1	43	37	6	2	...	395

fraction of SiCl₂ relative to SiCl. It should be noted that the uncertainty in the sputter yield for lower ion energies is expected to be greater due to the low absolute values of the sputter yield. The important role of Cl in sputtering is discussed in the next section of this article. Table II lists the sputter yield enhancement, defined as $S_e = Y(1\text{ML Cl-passivated Si})/Y(\text{bare Si})$ for various energies. Though the sputter yield enhancement for amorphized silicon is relatively low $S_e \leq 2.23$ for Ar ion energies down to 75 eV,

TABLE II. The energy and lattice dependence of the sputter yield enhancement $S_e = Y(1\text{ML Cl-passivated Si})/Y(\text{bare Si})$. $S_e \rightarrow \infty$ indicates perfect sputter enhancement control, suitable for ALET.

E (eV)	S_e (defect-free)	S_e (amorphous)
37.5		∞
50	∞	1.53
75	∞	2.23
120	3.94	1.55
200	2.14	1.53

perfect sputter yield enhancement control, $S_e \rightarrow \infty$, is observed at 37.5 eV, suggesting that at these low energies nearly ideal ALET is possible. S_e for defect-free silicon is observed to be higher than the amorphized Si enhancement factors, with perfect sputter enhancement control for Ar ion energies up to 75 eV.

Similar sputter enhancement has been observed in the MD study by Barone¹⁵ and Barone and Graves,³² and in an experimental study by Balooch *et al.*²⁹ for conditions with low chlorine surface coverage. It has been found that under low Cl surface coverage (≤ 1 ML), Cl does not mix below the Si surface,^{12,44} even after repeated argon bombardment^{12,13} or by 25 eV Cl^+ direct abstraction etching (DAE) simulations.^{14,15}

With increasing argon ion energy, larger clusters (Si_xCl_y , $x=2,3,4$) have been observed. However, these clusters appear mainly when chlorine is present. Only two Si dimer pairs have been observed to sputter in simulations where Cl is absent (see third row of 200 eV entry in Table I).

An issue to address is the degree of energy propagation within the lattice. With higher ion impact energies, deeper-penetrating cascades and argon penetration is expected. Under the conditions of this study, we have observed that (a) most product species are generated from the topmost silicon layer, and (b) product species are ejected well within the first 0.5 ps after impact. These findings suggest that chemical sputtering in the sense of Coburn and Winters⁴⁵ is not present, consistent with the results of Athavale and Economou¹² and Barone and Graves¹⁶ for low Cl/Ar ratios. Another observation is that for higher energy impacts, namely 75 and 120 eV, the nine atomic-layer lattice is not deep enough to contain the full cascade. However, this is not expected to affect the product formation. At 120 eV, several impacts resulted in product ejection following complicated sequences of cascade atom collisions, but involving atoms only within the top three silicon layers.

C. Reaction mechanisms

An important result arising from impacts on defect-free silicon is the observation and inference of clear and well-defined product formation mechanisms. These mechanisms are relevant in such processes as ALET in which the maintenance of an ordered lattice with minimal damage is required. With the use of well-characterized defect-free surface lattices, it has been observed in this study that product formation is influenced by surface atomic geometries and is strongly correlated to surface impact location within a surface unit cell. Similar correlations have been made in a study of defect formations^{18,19} as well as sputtering of Si with 1.5 keV Ar.⁴⁶

For a defect-free silicon system relevant to ALET, we found that the Si-containing product formation mechanisms are mainly of three different types, depending on the energetic species formed after the first collision of argon with the surface, i.e., recoiled Cl (Type (I)), recoiled Si (Type (II)) or scattered Ar (Type (III)). It is these “active” species which wedge between and beneath silicon atoms imparting upward momentum or creating an unstable surface state which even-

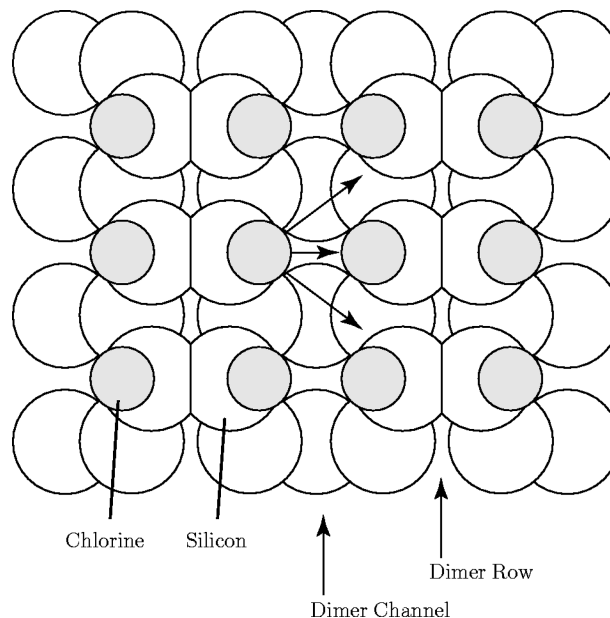


FIG. 6. Top view of a defect-free Cl-passivated $\text{Si}(001)(2 \times 1)$ surface (atoms are not drawn to scale). In the Type (I) mechanism, an energetic Cl recoil travels in one of the three directions shown across the dimer channel.

tually leads to product ejection. Although we only discuss these three main categories, other more complicated pathways are also observed, especially at higher energies ($E=120,200$ eV). From these mechanisms, only Type (II) can occur on bare Si surfaces, whereas all three types can occur on Cl-passivated surfaces. A more detailed description of product formation mechanisms can be found elsewhere.⁴⁷

In the Type (I) mechanism (Fig. 6), argon impact recoils a Cl such that the now energetic Cl travels laterally across the dimer “channel.” This energetic Cl bonds with the nearest silicon on the adjacent dimer row, or on one of the silicon atoms of a dimer pair next to the nearest silicon. A SiCl or SiCl_2 surface species is ejected depending on the energetic chlorine’s ability to attach to the target silicon and dissipate much of its kinetic energy to the surrounding lattice.

As an example, Fig. 7 shows snapshots of a representative simulation in which 50 eV Ar is impacted normally onto a defect-free Cl-passivated silicon $(001)(2 \times 1)$ surface. Some Cl atoms were removed from the images to provide a clearer view of the surface reaction. The reaction begins with Fig. 7(a), where the larger sphere represents the argon ion and the smaller darker and lighter spheres represent chlorine and silicon atoms, respectively. Figure 7(b) shows Ar colliding with a chlorine atom attached to a “dimer.” This collision takes place such that the Si–Cl “bond” is broken and the Cl is recoiled towards the dimer rows. The kinetic energy of the chlorine atom is approximately 10 eV when it travels directly across the channel in the adjacent dimer row as shown in Fig. 7(c). Approximately 0.18 ps after the initial argon impact, a SiCl_2 species desorbs with 1.13 eV kinetic energy (Fig. 7(d)).

In a reaction involving the Type (II) mechanism, an argon ion impacts the surface directly between a surface dimer pair. The dimer silicon atoms split and recoil in opposite

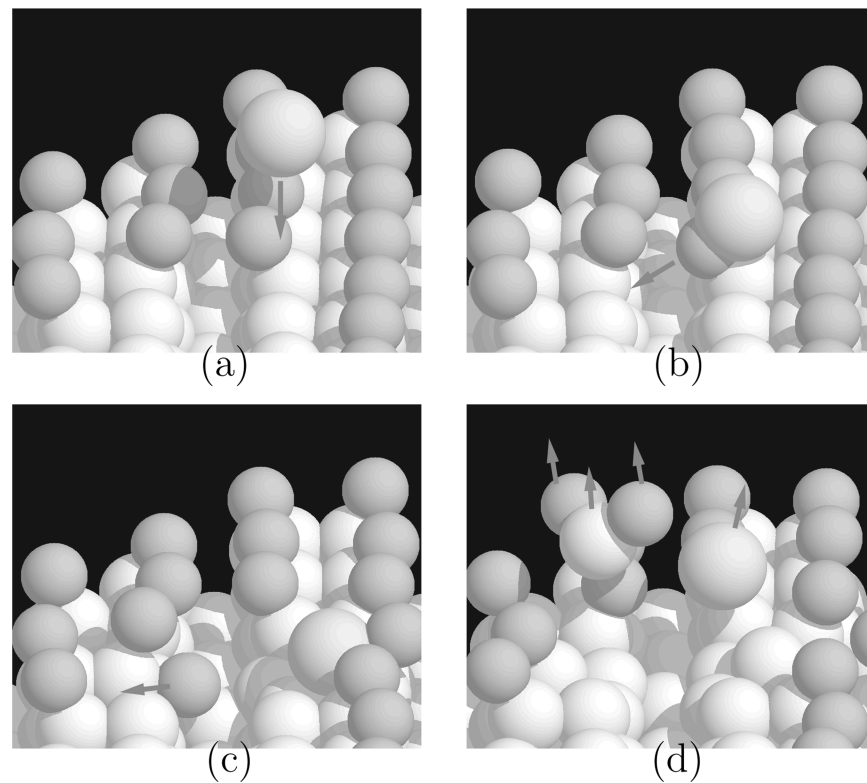


FIG. 7. Snapshots of a simulation representative of the Type (I) mechanism. Ar impacts normally onto the surface colliding with Cl (a). The Cl recoils across the dimer channel (b), and bonds with a Si (c). This metastable surface configuration causes desorption of a SiCl_2 molecule (d).

directions nearly perpendicular to the dimer rows. These energetic recoil atoms appear to slice beneath the dimer pairs in adjacent dimer rows, causing the ejection of SiCl_x , $x=0,1,2$ or Si_2Cl_y , $y=0,1,2,3$. A similar “dimer splitting” has been observed in a study by Kitabatake and Greene,¹⁸ though in their example with 50 eV silicon, sputtering did not occur. One interesting observation for Ar ion energy of 75 eV is the presence of the Type (II) mechanism in the Cl-passivated lattice and absence of this mechanism in the Cl-free lattice (as indicated by the lack of any observed sputtered products). This suggests that, at low ion impact energies, chlorine atoms play a role in the Si ejection process for this mechanism.

Figure 8 shows snapshots of a simulation in which 120 eV argon impacts a defect-free Cl-passivated silicon lattice. In Fig. 8(a), the Ar impacts the surface splitting the dimer, as shown in Fig. 8(b). These recoiled silicon atoms slice or cleave beneath the silicon directly across the dimer channel, as shown in Fig. 8(c). In Fig. 8(d), the right-hand recoiled silicon has enough kinetic energy to cleave the entire dimer, forming a Si_2Cl_2 product, while the other recoiled silicon produces only SiCl. Instances have been observed where the dimer product is unable to dissipate its internal energy causing it to dissociate into two SiCl_y species, $y=0,1$.

Finally, in reactions involving the Type (III) mechanism, the incident Ar atom scatters off a Cl atom, and is able to penetrate beneath a neighboring silicon causing the ejection of product species. This mechanism is not so well defined, in the sense that it does not follow one or few well-defined local trajectories as is observed with the Types (I) and (II) mechanisms.

An important result of this study is the correlation of initial impact location with sputtering, as well as particular surface reaction mechanisms. Figures 9 and 10 show scatter plots of initial Ar ion impact locations on Cl-free and Cl-passivated silicon surfaces, respectively, on an otherwise defect-free (2×1) unit cell. Each point represents the initial Ar position from a single simulation run which resulted in silicon-containing product species ejection. Figure 9(a) shows the clear dominance of the Type (II) mechanism for the simulations involving 120 eV Ar. In Fig. 10, the presence of adsorbed Cl provides a greater number of possible pathways in which Ar impacts lead to sputtered products. The prominence of Type (II) mechanism appears to increase with increasing energy, as well as the Type (III) mechanism, which is absent at 50 eV. Furthermore, for the Type (I) and Type (III) mechanisms, the Ar impact locations appear to localize in an arc region around the Cl, consistent with the descriptions of these mechanisms. Very few products are observed by direct impact onto dimer channel regions of the unit cell in this study. Apparently, the surface reconstruction leaves exposed “holes” in the surface allowing for a significant portion of the incident ions to undergo a primary impact with deeper silicon layers, decreasing the probability that sputtering will occur.⁴⁶

Figures 9(b) and 10(d) show the same impact-sputter correlation maps for 200 eV Ar ions on bare and Cl-passivated defect-free silicon, respectively. We have found that at this energy, the observed trajectories do not follow the three basic mechanism types discussed above, but rather, many different more complicated pathways. Thus mecha-

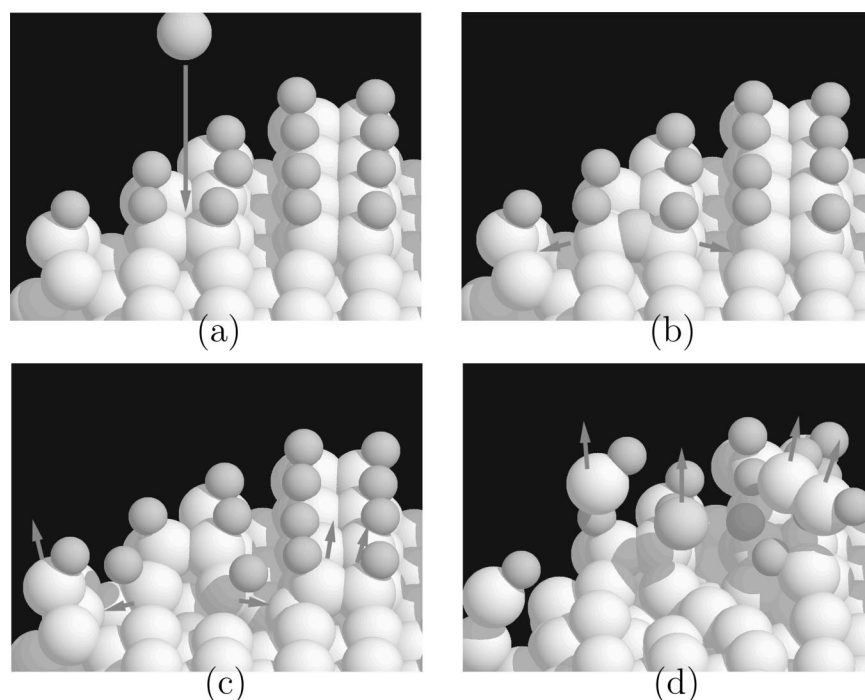


FIG. 8. Snapshots of a simulation representative of the Type (II) mechanism. Ar impacts the surface (a), and causes a Si dimer to split and recoil in opposite directions (b). These energetic Si atoms recoil across respective dimer channels and undercut the neighboring dimers (c). As a result, Si_2Cl_2 and SiCl molecules are ejected from the surface (d).

nisms were not distinguished in Figs. 9(b) and 10(d). A worthwhile observation is the significant departure from the localized impact regions, seen with lower energy impacts, to a more diffuse region around the surface dimer silicon atoms. For Ar impacting Cl-free ordered Si, a significant fraction of recoil Si and scattered Ar atoms is observed to cleave beneath the *second* layer silicon atoms resulting in the sputtering of these secondary silicon recoils. A similar correlation map of Stansfield *et al.*⁴⁶ for 1.5 keV Ar on Si shows a concentration of sputtering as a result of Ar impacting an arc

region in the irreducible symmetry zone of 2×1 reconstructed Si, similar to that in Fig. 9(b). The presence of Cl chemisorbed on the surface appears to isolate the sputtering to mainly the topmost silicon layer, which is a desirable result for the ALET process. This is shown in Table III which lists the fraction of silicon-containing product species originating from different layers of initially defect-free lattices. We should note at this point that for high enough ion energies, even a defect-free starting surface will eventually be amorphized. The correlation between ion impact location and sputter mechanism will then be difficult to obtain. Although ion energies that result in excessive surface amorphization are not suitable for ALET, results for such energies are still included here for completeness.

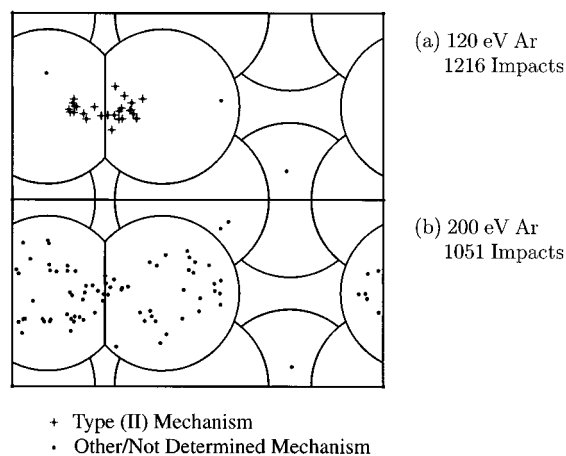


FIG. 9. Top view of a surface unit cell of a defect-free bare $\text{Si}(001)(2 \times 1)$ surface. The points represent initial (a) 120 eV and (b) 200 eV argon impact positions on the lattice which resulted in ejection of Si-containing product species. A total of 1216 and 1051 argon ions were impacted onto the surface for the 120 and 200 eV cases, respectively.

IV. CONCLUSIONS

The power of parallel computation has enabled the systematic study of very low-yield sputtering of solid surfaces. Extensive molecular dynamics simulations of argon ion impacts on silicon provide a great deal of information about the nature of sputtering at low energies. The sputter yield of silicon is found to agree well with available experimental and other simulation data. The yield is found to be essentially zero below 37.5 eV. The presence of chlorine on the surface is found to increase the yield at all ion energies. As the Cl-surface coverage increases, the sputter yield follows a generally increasing trend. Important product ejection pathways are identified relevant to atomic layer etching (ALET), using argon ion impacts on defect-free silicon covered with a ML of chlorine. As the ion energy increases, the number and complexity of the various pathways also increases. Higher energy impacts provide not only the energy to break more

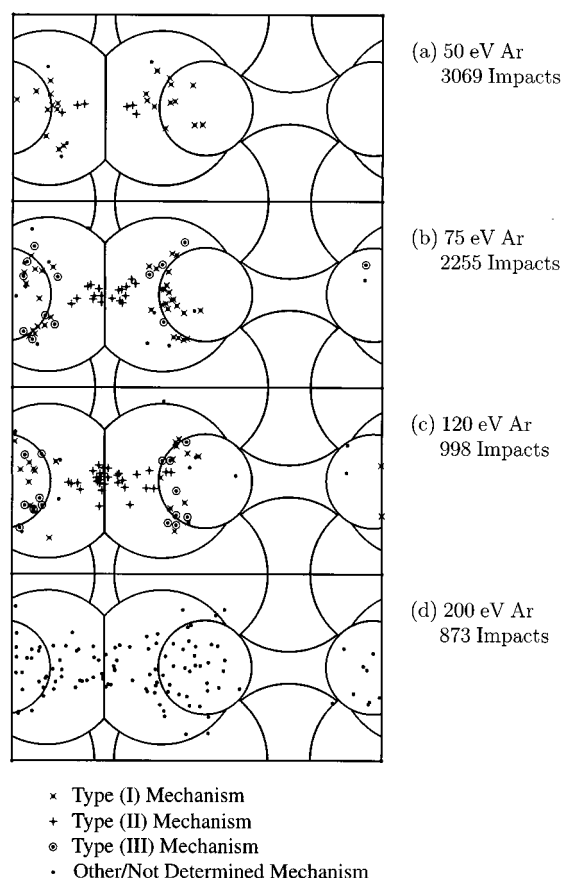


FIG. 10. Top view of a surface unit cell of a defect-free Cl-passivated Si (001)(2×1) surface. The points represent initial (a) 50 eV, (b) 75 eV, (c) 120, and (d) 200 eV argon impact positions on the lattice which resulted in ejection of Si-containing product species. A total of 3069, 2255, 998 and 873 argon ions were impacted onto the surface for cases (a), (b), (c), and (d), respectively.

bonds and produce larger collision cascades, but they also sustain a higher temperature “hot-spot” providing the necessary energy to eject metastable surface species. Furthermore, the higher energy impacts involve collisions and sput-

TABLE III. Origin of silicon-containing sputtered product species by silicon layer number. L=1 indicates the topmost silicon layer. P=pristine lattice.

E (eV)	Lat.	(ML)	L=1	L=2	L=3
50	P	0	1.000
50	P	1	1.000
75	P	0	1.000
75	P	1	1.000
120	P	0	0.933	0.033	0.033
120	P	1	0.990	0.010	...
200	P	0	0.488	0.429	0.083
200	P	1	0.913	0.060	0.027

tering of silicon atoms below the topmost silicon layer. Such events are undesirable for processes which require etching with monolayer accuracy such as ALET.

ACKNOWLEDGMENTS

Special thanks to Dr. Maria Barone and Dr. John Daugherty at Lam Research Corporation, Dr. Richard Wise at IBM and Dr. Karanam Srinivasa Rao at the University of Houston for their helpful and greatly informative discussions. Also, many thanks to Dr. Roger A. Sayle of Glaxo Wellcome Medicines Research Centre for his invaluable assistance with RasMol³⁹ visualization, and to Dr. Raj Rajagopalan at the University of Houston for providing video equipment for recording of animations. Computational resources have been generously provided by the Massively Parallel Computation Research Laboratory (MPCRL) of Sandia National Laboratory. This work was supported financially by the National Science Foundation (CTS-9713262) and the State of Texas through the Texas Advanced Technology Program.

- ¹T. Matsuura, K. Suzue, J. Murota, Y. Sawada, and T. Ohmi, *Appl. Phys. Lett.* **63**, 2803 (1993).
- ²S. Athavale and D. J. Economou, *J. Vac. Sci. Technol. B* **14**, 3702 (1996).
- ³T. Ishii, K. Meguro, T. Gamo, T. Sugano, and Y. Aoyagi, *Jpn. J. Appl. Phys., Part 1* **32**, 6178 (1993).
- ⁴T. Meguro, M. Ishii, K. Kodama, Y. Yamamoto, K. Gamo, and Y. Aoyagi, *Thin Solid Films* **225**, 136 (1993).
- ⁵Y. Aoyagi, K. Shinmura, K. Kawasaki, I. Nakamoto, K. Gamo, and S. Namba, *Thin Solid Films* **225**, 120 (1993).
- ⁶K. K. Ko and S. W. Pang, *J. Vac. Sci. Technol. B* **11**, 2275 (1993).
- ⁷D. L. Bourne, D. Hart, D. M. Rayner, and P. Hackett, *J. Vac. Sci. Technol. B* **11**, 556 (1993).
- ⁸M. A. Lieberman and A. J. Lichtenberg, *Principles of Plasma Discharges and Materials Processing* (Wiley, New York, 1994).
- ⁹J. W. Coburn and H. F. Winters, *J. Appl. Phys.* **50**, 3189 (1979).
- ¹⁰T. Mizutani, C. J. Dale, W. K. Chu, and T. Mayer, *Nucl. Instrum. Methods Phys. Res. B* **3**, 825 (1985).
- ¹¹D. J. Oostra, A. Haring, R. P. van Ingen, and A. E. de Vries, *J. Appl. Phys.* **64**, 315 (1988).
- ¹²S. D. Athavale and D. J. Economou, *J. Vac. Sci. Technol. A* **13**, 966 (1995).
- ¹³H. Feil, J. Dieleman, and B. J. Garrison, *J. Appl. Phys.* **74**, 1303 (1993).
- ¹⁴M. E. Barone, T. O. Robinson, and D. B. Graves, *IEEE Trans. Plasma Sci.* **24**, 77 (1996).
- ¹⁵M. E. Barone, Ph.D. thesis, University of California at Berkeley, 1995.
- ¹⁶M. E. Barone and D. B. Graves, *J. Appl. Phys.* **77**, 1263 (1995).
- ¹⁷B. A. Helmer and D. B. Graves, *J. Vac. Sci. Technol. A* **15**, 2252 (1997).
- ¹⁸M. Kitabatake and J. E. Greene, *J. Appl. Phys.* **73**, 3183 (1993).
- ¹⁹M. V. R. Murty and H. A. Atwater, *Phys. Rev. B* **45**, 1507 (1992).
- ²⁰E. L. Hu, C.-H. Chen, and D. L. Green, *J. Vac. Sci. Technol. B* **14**, 3632 (1996).
- ²¹R. J. Davis, A. Climent, and S. J. Fonash, *Nucl. Instrum. Methods Phys. Res. B* **7/8**, 831 (1985).
- ²²D. J. Vitkavage, C. J. Dale, W. K. Chu, T. G. Finstaad, and T. M. Mayer, *Nucl. Instrum. Methods Phys. Res. B* **13**, 313 (1986).
- ²³M. Ishii, Y. Hirose, T. Sato, T. Ohwaki, and Y. Taga, *J. Vac. Sci. Technol. A* **15**, 820 (1997).
- ²⁴P. Sigmund, *Phys. Rev.* **184**, 383 (1969).
- ²⁵R. Behrisch, *Sputtering by ion bombardment: Theoretical concepts*, Topics in Applied Physics (Springer, Berlin, 1981).
- ²⁶P. C. Zalm, *J. Vac. Sci. Technol. B* **2**, 151 (1984).
- ²⁷C. Steinbrüchel, *Appl. Phys. Lett.* **55**, 1960 (1989).
- ²⁸D. N. Ruzic, in *Handbook of Plasma Processing Technology: Fundamentals, Etching, Deposition, and Surface Interactions*, edited by S. M. Rossnagel, J. J. Cuomo, and W. D. Westwood (Noyes, Park Ridge, New Jersey, 1990), Chap. 3, pp. 70–90.
- ²⁹M. Balooch, M. Moalem, W.-E. Wang, and A. V. Hamza, *J. Vac. Sci. Technol. A* **14**, 229 (1996).
- ³⁰T. A. Schoolcraft and B. J. Garrison, *J. Am. Chem. Soc.* **113**, 8221 (1991).

- ³¹T. A. Schoolcraft, A. M. Diehl, A. B. Steel, and B. J. Garrison, *J. Appl. Phys.* **13**, 1861 (1995).
- ³²M. E. Barone and D. B. Graves, *J. Appl. Phys.* **78**, 6604 (1995).
- ³³H. J. C. Berendsen, J. P. M. Postma, W. F. van Gunsteren, A. DiNola, and J. R. Haak, *J. Chem. Phys.* **81**, 3684 (1984).
- ³⁴F. H. Stillinger and T. A. Weber, *Phys. Rev. B* **31**, 5262 (1985).
- ³⁵F. H. Stillinger and T. A. Weber, *J. Chem. Phys.* **88**, 5123 (1988).
- ³⁶F. H. Stillinger and T. A. Weber, *Phys. Rev. Lett.* **62**, 2144 (1989).
- ³⁷W. C. Swope, H. C. Andersen, P. H. Berens, and K. R. Wilson, *J. Chem. Phys.* **76**, 637 (1982).
- ³⁸R. Smith, D. E. J. Harrison, and B. J. Garrison, *Phys. Rev. B* **40**, 93 (1989).
- ³⁹R. A. Sayle, *RasMol Molecular Graphics Visualization Tool*, Glaxo Research and Development, Biomolecular Structures Group, 1994.
- ⁴⁰W. D. Leudtke and U. Landman, *Phys. Rev. B* **40**, 1164 (1989).
- ⁴¹D. J. Oostra, R. P. van Ingen, A. Haring, A. E. de Vries, and G. N. A. van Veen, *Appl. Phys. Lett.* **50**, 1506 (1987).
- ⁴²P. C. Zalm, *J. Appl. Phys.* **54**, 2660 (1983).
- ⁴³J. P. Chang, J. C. Arnold, G. C. H. Zau, H.-S. Shin, and H. H. Sawin, *J. Vac. Sci. Technol. A* **15**, 1853 (1997).
- ⁴⁴C. K. Ong and L. P. Tay, *J. Phys.: Condens. Matter* **1**, 1071 (1989).
- ⁴⁵J. W. Coburn and H. F. Winters, *Nucl. Instrum. Methods Phys. Res. B* **27**, 243 (1987).
- ⁴⁶R. A. Stansfield, K. Broomfield, and D. C. Clary, *Phys. Rev. B* **39**, 7680 (1989).
- ⁴⁷N. A. Kubota, Ph.D. thesis, University of Houston, Department of Chemical Engineering (unpublished).